

DETECTION OF GRAVITY WAVES ON MARS USING THEMIS BAND 10.

J. M. Battalio, *Dept. of Earth and Planetary Sciences, Yale University, New Haven, CT (joseph.battalio@yale.edu)*,
N. Heavens, **A. Pankine**, *Space Science Institute, Boulder, CO*, **J. Cowart**, *Dept. of Geosciences, Stony Brook University, Stony Brook, NY*.

Introduction

Atmospheric gravity waves (GW) emerge from disturbances in a stably stratified air mass and are restored by buoyancy¹. GWs control many processes found throughout all atmospheric layers so are extremely important for understanding the dynamics occurring in each layer, for capturing the coupling between the near-surface and the highest levels of planetary atmospheres, and for closing energy and momentum budgets of the general circulation². GWs are important for understanding atmospheric dynamics on Mars because they impact atmospheric escape processes, and as shown by Curiosity, they may instigate cloud activity³.

Recently, Heavens et al., (2020, 2022)^{4,5} developed a climatology of GWs from the Mars Climate Sounder (MCS). However, MCS can only look for GWs in the meridional direction; it cannot detect GWs in the zonal direction. To look for GW in the zonal direction, an imager can be used, like the Thermal Emission Imaging System (THEMIS). Specifically, we use Band-10, which has a weighting function that peaks at about 25 km above the surface, to search for GW activity in both the meridional and zonal directions. THEMIS has been in orbit on Mars Odyssey for two decades, yielding hundreds of thousands of image swaths. We focus on a season that overlaps with the brief time that MCS took nadir observations, $L_s=120^\circ-150^\circ$. Here, we summarize an analysis of GW activity from THEMIS observations over Mars years (MY) 26–33⁶.

THEMIS Band 10

The THEMIS instrument consists of a set of two cameras that image Mars at thermal-infrared and visible wavelengths⁷. The IR camera images across ten spectral filters between 6.5 and 14.88 μm , and the visible images between 0.45 and 0.85 μm . We diagnose GW activity on Mars using only THEMIS Band 10 observations. We focus on THEMIS Band 10 because it is centered on the CO₂ absorption band at 14.88 μm , so emission predominantly comes from the atmosphere.

THEMIS images are 320 pixels across-track and have a spatial resolution of ~ 100 m/pixel, with a width of 32 km. Images are taken in the along-track direction due to spacecraft motion and vary in length from ~ 30 km to hundreds of km, depending on the scientific motivation for a specific observation.

As Mars Odyssey maintains a Sun-synchronous orbit, images are captured twice a sol between 3:00 and 7:30 AM/PM depending on year and time of year. For $L_s=120^\circ-150^\circ$, observations during MYs 26–28 occurred around 5:00, migrated to 4:00 for 29–31, and then shifted to 7:00 for MY 33⁸.

Dataset Calibration

Bands 1–9 of each THEMIS image swath undergo a multi-step calibration pipeline before GW activity is calculated. However, the calibration for bands 1–9 is performed assuming that Band 10 is thermally homogeneous across the imaging scene, and Band 10 is left unaltered so that the calibration is reversible for other bands. GW activity invalidates this assumption, so the calibration must be performed for Band 10 separately from data on the PDS.

After converting the THEMIS RDR files into ISIS3 format (Fig. 1, Raw Swath), each image cube has band-dependent row and line correlated noise removed via the DaVinci “deplaid” and “destreak” functions⁹ (Fig. 1, Destreak & Deplaid). Time-dependent focal plane variations due to long-period thermal variation are removed¹⁰, similar to the “uddw” (UnDrift-DeWobble) DaVinci function but implemented for THEMIS Band 10. The Band 10 implementation necessitates a longer 1x400 boxcar filter (Fig. 1, Undrift & Dewobble). Temperature variations across the calibration flag are removed, similar to the “rtilt” DaVinci function⁹. An additional deplaid is applied to remove the band-independent Band 10 noise (Fig. 1, Rtilt & Deplaid). An additional set of destreak filtering is applied to remove several columns that are particularly oversaturated in Band 10. Each swath is sinusoidally map projected. Finally, swaths are binned at 1 km to improve the signal to noise.

Calculation of Gravity Wave Spectra

GW activity is calculated along multiple, unique baselines across each THEMIS Band 10 swath. To select the baselines, points are taken every 16 km in the cross-track direction and every 32 km in the along-track direction on swath edges. This establishes a 16×32 km grid of points. A line is swept 180° through each point, and the unique intersections generate the baselines on which GW activity is calculated. The 180° sweep constitutes the various orientations that GW activity can take, because the direction of wave propagation cannot be determined from a single swath. This results from spacecraft motion \gg wave phase speed, so each swath is considered instantaneous. The baseline length varies from 32 km to $\sim 2,000$ km, constrained by the swath dimensions.

For each baseline, GW activity is estimated following Heavens et al., (2020)⁴. The variance of the GW is estimated from the brightness temperature measurement^{11,12}, which is calculated from the retrieved Band 10 radiance. To account for differences in average temperature, the GW variance in an observation is normalized by the mean of the squared temperature in each measurement within the observation. This is denoted as $\hat{\Omega}_{GW}$,

THEMIS Gravity Waves

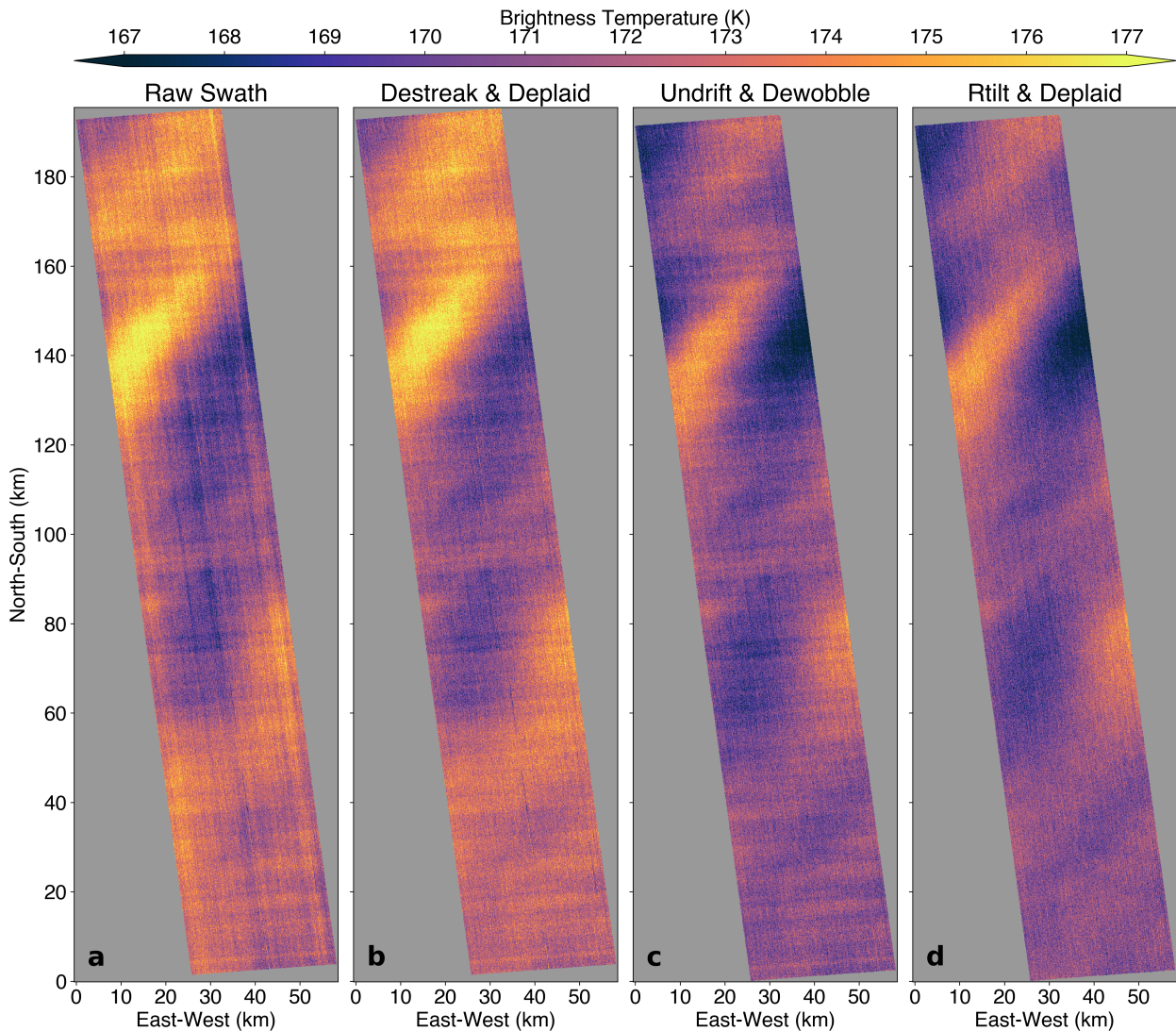


Figure 1: Sequence of the pre-processing steps for THEMIS band 10 swath (I55019007) at $L_s=128.8^\circ$, MY 32 which occurs at 297.7°E , $40.2\text{--}43.3^\circ\text{S}$. To show each step, the swaths are each sinusoidally projected, but the preprocessing is all performed before map projection. Gray shading indicates areas outside of the swath. Adapted from Battalio et al., (submitted)⁶.

with units $K^2 K^{-2}$. The associated GW activity variance is binned for length-orientation on each baseline every $1 \text{ km} \times 2^\circ$. All swaths with length $> 70 \text{ km}$ are subset into multiple trapezoids of size $\sim 32 \times 32 \text{ km}$, and the GW activity procedure is repeated on them. These are called “symmetric” swaths.

Each THEMIS swath has an associated unique GW spectrum, and the above method robustly identifies the main GW modes. The swath calibrated in Fig. 1 has several GW modes superimposed, and the average spectrum captures each (Fig. 2a). The spectrum is binned by 1 km of baseline and by 2° of orientation. The spectral peaks above the mean are indicated and numbered in decreasing amplitude. For sufficiently long swaths, a particular baseline (length, orientation) bin may contain multiple baselines; these are averaged together. By inspection, there are at least three GW peaks denoted by the dashed lines in Fig. 2a: a 20 km baseline GW with

-70° orientation (black, dashed lines), a 30 km baseline wave with -50° orientation (red, dashed lines), and an 80 km baseline wave with 50° orientation (red, dashed lines). The average spectrum (Fig. 2b) exhibits a peak for each of these modes.

Average Gravity Wave Activity

GW activity exhibits several overarching patterns (Fig. 3a,d). Activity maximizes near the southern polar cap, poleward of 60°S both during the day (Fig. 3a) and night (Fig. 3d), greater than $\log_{10}(\hat{\Omega}_{GW}) = -5 \text{ K}^2 \text{ K}^{-2}$. Within this zonal band of greatest activity, there is some longitudinal localization at $150^\circ\text{--}100^\circ\text{W}$ and $30^\circ\text{--}70^\circ\text{E}$, to the east of the large Argyre and Hellas basins. Outside of this zonal band, GW activity is reduced in the equatorial regions, particularly at night, and there is low activity throughout the northern hemisphere.

THEMIS Gravity Waves

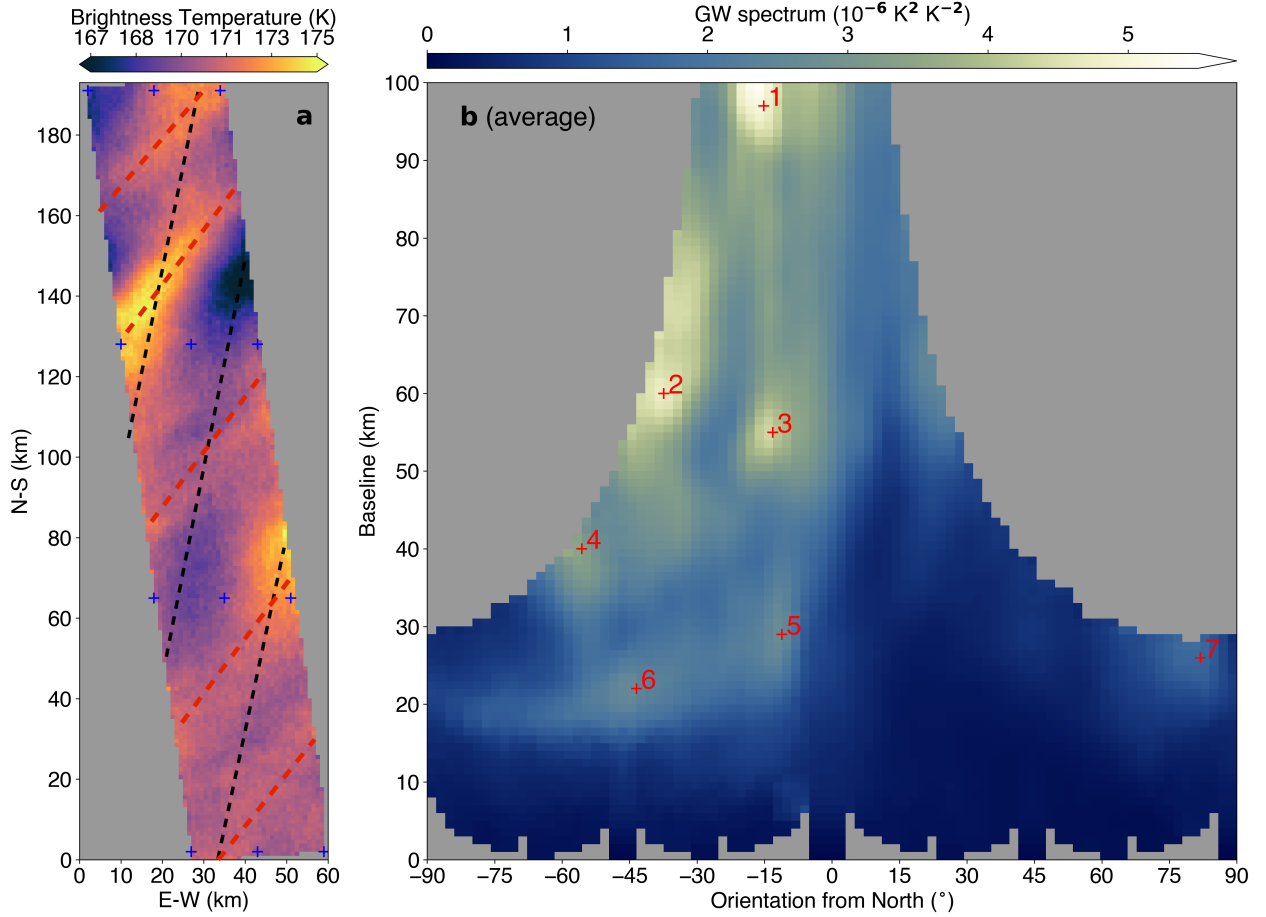


Figure 2: The THEMIS band 10 swath processed in Fig. 1 binned at 1 km resolution (a) and the associated average GW spectrum binned every 1 km of baseline by 2° or orientation (b). Blue crosses indicate locations defining baseline sweeps, and dashed lines denote GW fronts in (a), and numbers indicate the spectral peaks in (b). Gray shading indicates a lack of data. Adapted from Battalio et al., (submitted)⁶.

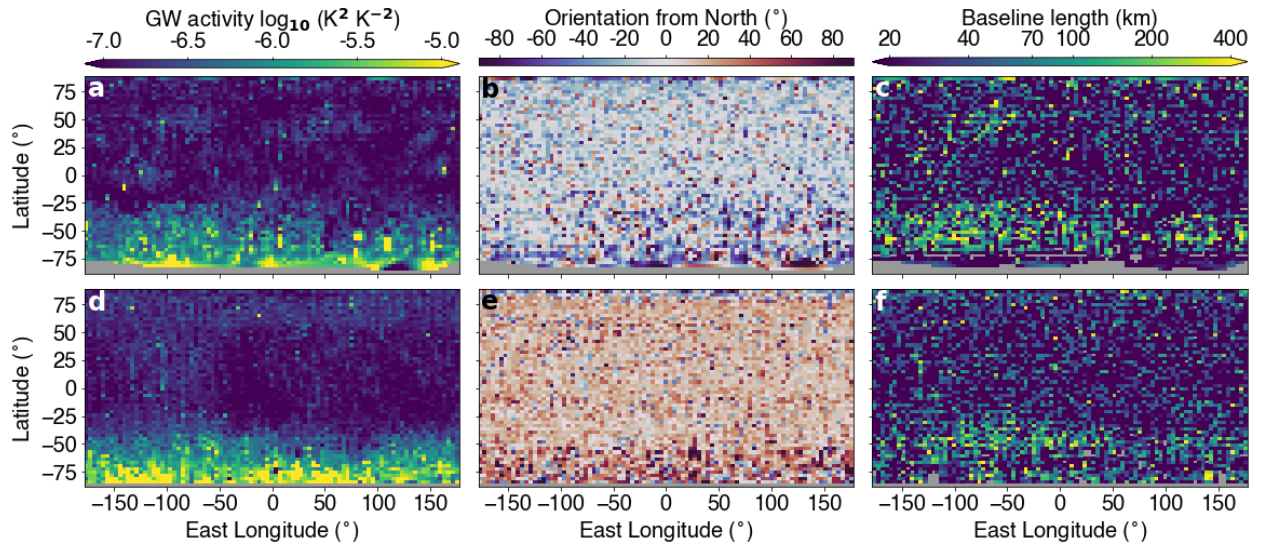


Figure 3: Peak GW activity ($\log_{10} \hat{\Omega}_{GW} \text{ K}^2 \text{ K}^{-2}$) (a,d), orientation (deg from north-south) (b,e), and baseline length (km) (c,f) for all THEMIS GW observations during $L_s = 120^\circ - 150^\circ$, MY 26-33 binned at the median at 4° resolution. Daytime observations (a-c) and nighttime observations (d-f). Gray shading indicates lack of observations. Adapted from Battalio et al., (submitted)⁶.

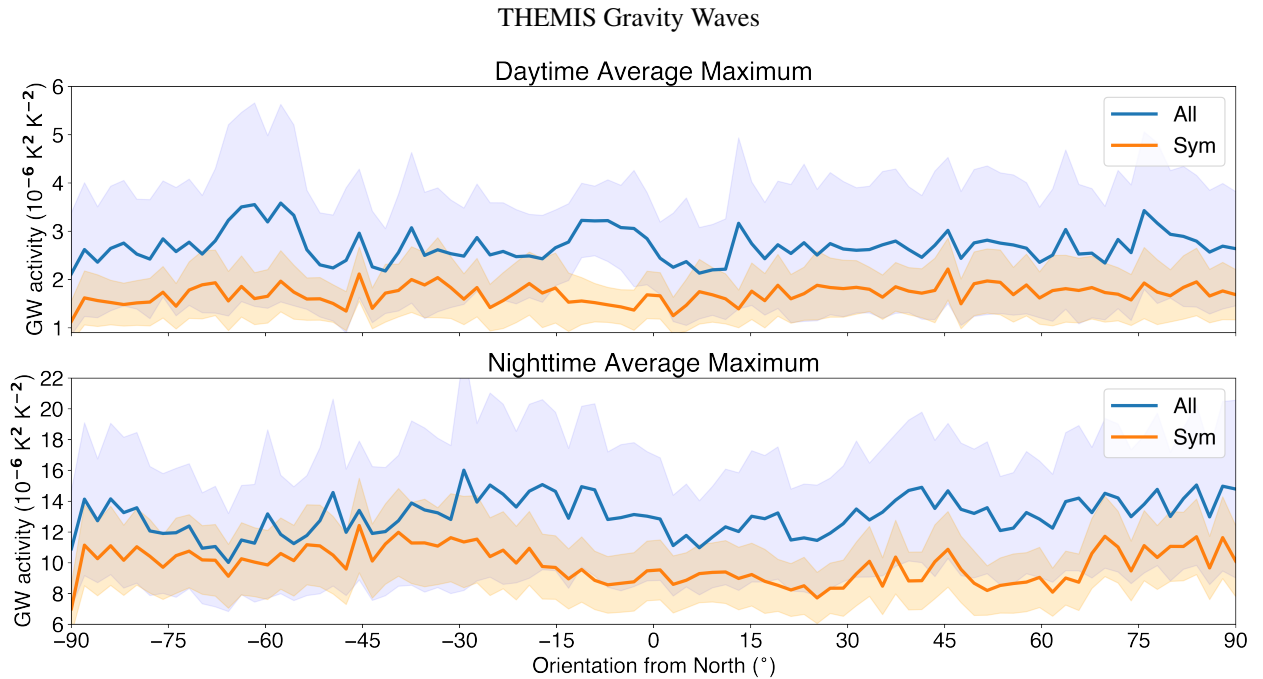


Figure 4: Average GW activity maximum at a particular orientation for the day (top) and night (bottom) for all complete THEMIS swaths (blue) and for all swath subsets (orange). Shading indicates standard deviation. Adapted from Battalio et al., (submitted)⁶.

There is considerable variance in the approximate wavelength of the GWs, measured as the length of the baseline. The shortest observed wavelengths of less than 40 km are near the southern pole, both at day (Fig. 3c) and night (Fig. 3f); however, daytime wavelengths are shorter than nighttime. The longest lengths of greater than 100 km are found just to the north, collocated with the highest latitudinal gradients of GW activity along 60°S. Outside of these areas, there is little organization of the baseline lengths at night.

The average GW orientation is generally north-south, northward of the greatest activity along 60°S, both during the day (Fig. 3b) and night (Fig. 3e), though the activity is somewhat west of due north at night and somewhat east of due north at day by approximately 10°. This effect is an observational bias in the data caused by the trajectory of Odyssey in its sun-centric orbit, which is south to north during the day and north to south at night.

Despite this bias, GWs during $L_s=120^\circ-150^\circ$ are isotropic, meaning that no particular orientation is favored when considering observations at all spatial locations both during the day (Fig. 4, top) and night (Fig. 4, bottom). For both symmetrically subdivided swaths (Fig. 4, orange) and even for the full swath lengths (Fig. 4, blue), activity is not distinguishable from a constant value across all orientations. This shows that despite biases from spacecraft motion, the method of evaluating GW activity by rotating through all baselines is robust.

Summary

Gravity waves on Mars contribute to atmospheric escape, impact cloud formation, and provide an impor-

tant mechanism for energy and momentum transport. With increasing complexity of gravity wave parameterizations used by Mars global circulation models, the development of complete gravity wave datasets is crucial for model verification. Until now, many gravity wave climatologies have used instrumentation sensitive to waves oriented only in the meridional direction, missing activity oriented zonally. To remedy this coverage gap, gravity waves are analyzed from THEMIS Band 10 over approximately one Mars month, totaling >30,000 spectra. Gravity wave activity exhibits an isotropic distribution among wavelengths detectable in all directions (<20 km). In directions sensitive to longer wavelengths, activity at shorter baselines remains the most prominent. Activity peaks near the southern pole, at appreciably longer wavelengths (~100–200 km).

Acknowledgments

This work was funded by NASA's Mars Data Analysis Program (80NSSC19K1215).

REFERENCES: [1] Fritts et al. 2003, Rev. of Geophys., 41, 1. [2] Medvedev et al. 2019, Atmosphere, 10, 531. [3] Guzewich et al. 2021, JGR: P, 126. [4] Heavens et al. 2020, Icarus, 341, 113630. [5] Heavens et al. 2022, PSJ, 3. [6] Battalio et al. submitted, JGR: P. [7] Christensen et al. 2004, Space Science Reviews, 110, 85. [8] Smith, M. D. 2019, Icarus, 333, 273. [9] Edwards et al. 2011, JGR: P, 116, 1. [10] Banfield et al. 2004, Icarus, 170, 365. [11] Wu et al. 1996, GRL, 23, 3289. [12] Wu et al. 1996, GRL, 23, 3631.